**Cell Death &
Differentiation**

ARTICLE

CBFβ promotes colorectal cancer progression through transcriptionally activating OPN, FAM129A, and UPP1 in a RUNX2-dependent manner

Chen Wang [1] · Ziyu Shi[1] · Yuqian Zhang[1] · Mingyue Li[1] · Jie Zhu[1] · Zhen Huang [1] · Junfeng Zhang [1] ·
Jiangning Chen [1,2]

Abstract

Colorectal cancer (CRC) is commonly associated with aberrant transcription regulation, but characteristics of the dysregulated transcription factors in CRC pathogenesis remain to be elucidated. In the present study, core-binding factor β (CBFβ) is found to be significantly upregulated in human CRC tissues and correlates with poor survival rate of CRC patients. Mechanistically, CBFβ is found to promote CRC cell proliferation, migration, invasion, and inhibit cell apoptosis in a RUNX2-dependent way. Transcriptome studies reveal that CBFβ and RUNX2 form a transcriptional complex that activates gene expression of OPN, FAM129A, and UPP1. Furthermore, CBFβ significantly promotes CRC tumor growth and live metastasis in a mouse xenograft model and a mouse liver metastasis model. In addition, tumor-suppressive miR-143/145 are found to inhibit CBFβ expression by specifically targeting its 3′-UTR region. Consistently, an inverse correlation between miR-143/miR-145 and CBFβ expression levels is present in CRC patients. Taken together, this study uncovers a novel regulatory role of CBFβ-RUNX2 complex in the transcriptional activation of OPN, FAM129A, and UPP1 during CRC development, and may provide important insights into CRC pathogenesis.

Introduction

Colorectal cancer (CRC) is one of the most prevalent cancer types worldwide, and liver metastasis ranks as the leading cause of CRC-related death [1]. Previous studies have extensively shown that genetic and epigenetic alterations critically contribute to CRC pathogenesis and progression [2]. Dysregulation of transcriptional factors such as β-catenin, which lead to tumor-related gene expression modifications and intracellular regulatory network disorders, are key determinants in CRC [3]. Recently, Homeobox protein Hox-B13 (HOXB13) is demonstrated to suppress C-myc expression and exert antitumor effects via β-catenin/TCF4 signal in CRC, which correlates with good prognosis of CRC patients [4]. High expression of myocyte enhancer factor 2D (MEF2D) correlates with metastatic process and poor prognosis of CRC patients, and has been proven to activate ZEB1 transcription and promote cell invasion and epithelial mesenchymal transition (EMT) [5]. Therefore, understanding the mechanisms of dysregulated transcriptional factors remains important in improving survival rate of CRC patients.

Core-binding factor is a heterodimeric transcriptional factor consisting of the DNA-binding α subunit (also called Runt-related transcription factor, RUNX) and the non-DNA-binding β subunit (CBFβ). The RUNX family has three members, RUNX1, RUNX2, and RUNX3. Upon dimerization, the CBFβ-RUNX heterodimeric complex undergoes a structural change, thereby achieving high DNA-binding affinity and stability [6]. Then, the complex regulates the expression of its target genes involved in a variety of physiological processes, such as

haematopoietic maturation and bone formation [7, 8]. Evidence has shown that CBFβ is essential for prostate and ovarian cancer cell growth, and breast cancer cell invasion [9, 10]. However, the role of CBFβ in CRC is not fully understood. In addition, reasonable attention has also been directed to the RUNX genes because of their prominent roles in cancer pathogenesis: they can function either as oncogenic genes or cancer suppressor genes, depending on the contexts of different cancers [11, 12]. The oncogenic role of RUNX2 has been identified in osteosarcoma [13], pancreatic cancer [14], and lymphoma [15]. RUNX2 is identified as an epigenetic regulator of EMT by integrative multiomics analysis in colon cancer cell lines [16]. RUNX2 deletion in CRC cells by small interfering RNA (siRNA) significantly decreased CRC cell proliferation and migration [17]. Downregulated RUNX1 promotes breast cancer development in hormone-negative breast cancers that lack human epidermal growth factor receptor 2 amplification [18]. *Runx1* deficiency enhances intestinal tumorigenesis in Apc^{Min} mice [19]. A lack of RUNX3 function leads to the EMT-like changes in hepatocellular carcinoma as well as gastric epithelial cell proliferation [20, 21]. RUNX3 gene inactivation and RUNX3 protein mislocalization have been recognized as the precancerous events of CRC [22]. RUNX3 exerts tumor suppressor effect by attenuating β-catenin/TCF4 in intestinal tumorigenesis [23]. RUNX3 also suppresses cell growth by inhibiting c-Myc in CRC [24]. However, little is known about CBFβ action and its downstream effectors in CRC.

In the present study, increased CBFβ expression is found to be closely associated with poor survival rate of CRC patients. In vivo data suggest that CBFβ can promote CRC tumor growth and liver metastasis. Mechanistically, CBFβ promotes CRC cell proliferation, migration, invasion, and inhibits CRC cell apoptosis through forming transcriptional complex with RUNX2 that activates the transcription of multiple oncogenic genes including OPN, FAM129A, and UPP1. Furthermore, miR-143/145 are identified to inhibit CBFβ expression by specifically targeting its 3′-UTR region, which results in the upregulation of CBFβ expression in CRC patients. These results suggest that CBFβ acts as a transcriptional factor to promote CRC progression through activating gene expression of OPN, FAM129A, and UPP1 in a RUNX2-dependent manner, thereby providing important insights into CRC pathogenesis.

Results

Upregulation of CBFβ expression correlates with overall survival in CRC

To investigate the clinical relevance of CBFβ expression in CRC, immunohistochemistry (IHC) was applied to a commercial tissue microarray (TMA) taken from a cohort of 180 CRC patients. CBFβ was localized in both the nucleus and cytoplasm of tumor cells, and significantly higher expression levels of CBFβ were observed in CRC tissues than in normal adjacent tissues (NAT) (Fig. 1A, B). The results of TMA indicated that 124 cases (68.9%) showed high expression of CBFβ (IRS ≥ 8), and 56 cases (31.1%) showed low expression of CBFβ (IRS < 8). As shown in Fig. 1C and Table S1 (Supporting Information), the CBFβ level in CRC tissues was associated with the differentiation state of CRC cells ($p = 0.0063$), tumor size ($p = 0.0257$), and lymphatic metastasis ($p = 0.0102$) but not sex or age, as determined by the χ^2 test. In addition, CRC patients with high CBFβ expression had a shorter 9-year overall survival of 61.25% using the Kaplan–Meier method. In contrast, the overall survival rate was 71.90% for CRC patients with low CBFβ levels ($p = 0.0110$) (Fig. 1D). Western blot analysis confirmed that the expression level of CBFβ in 54 CRC tissues was significantly higher than that in NAT (Fig. 1E, F and Table S2, Supporting Information). These results indicated that CBFβ upregulation is a common event in CRC tissues, which may be involved in CRC development.

RUNX1-3 expression in CRC patients

To exert specific functions, CBFβ requires its partner RUNX to confer DNA-binding activity. Thus, the roles of RUNX1, 2, and 3 in CRC were investigated in the following analyses. The protein levels of RUNX1, RUNX2, or RUNX3 were examined by IHC on a TMA from a cohort of 75 CRC patients. The IHC results indicated that RUNX1 and RUNX3 protein levels were downregulated in CRC tissues compared with NAT, while the protein level of RUNX2 was upregulated in CRC tissues (Fig. 2A, B; for patient information, refer to Table S3, Supporting Information). Western blot results in 10 paired CRC tissues and NAT showed the same trends in the expression of RUNX1, RUNX2, and RUNX3 examined by IHC (Fig. 2C, D; for patient information, refer to Table S4, Supporting Information). These data suggest that CBFβ may play an oncogenic role through interacting with RUNX2 rather than RUNX1 and RUNX3 in CRC.

CBFβ promotes CRC cell proliferation, migration, invasion, and inhibits cell apoptosis in a RUNX2-dependent manner

To study the biological function of CBFβ, stable HCT116 and SW480 cells with CBFβ overexpression (CBFβ-LV) or CBFβ knockdown (shRNA-CBFβ-LV) and their control cells (Control-LV/shRNA-Control-LV) were constructed. The overexpression and knockdown efficiency were confirmed by real-time PCR and western blot analysis in HCT116 and SW480 cells (Fig. S1A, B, Supporting
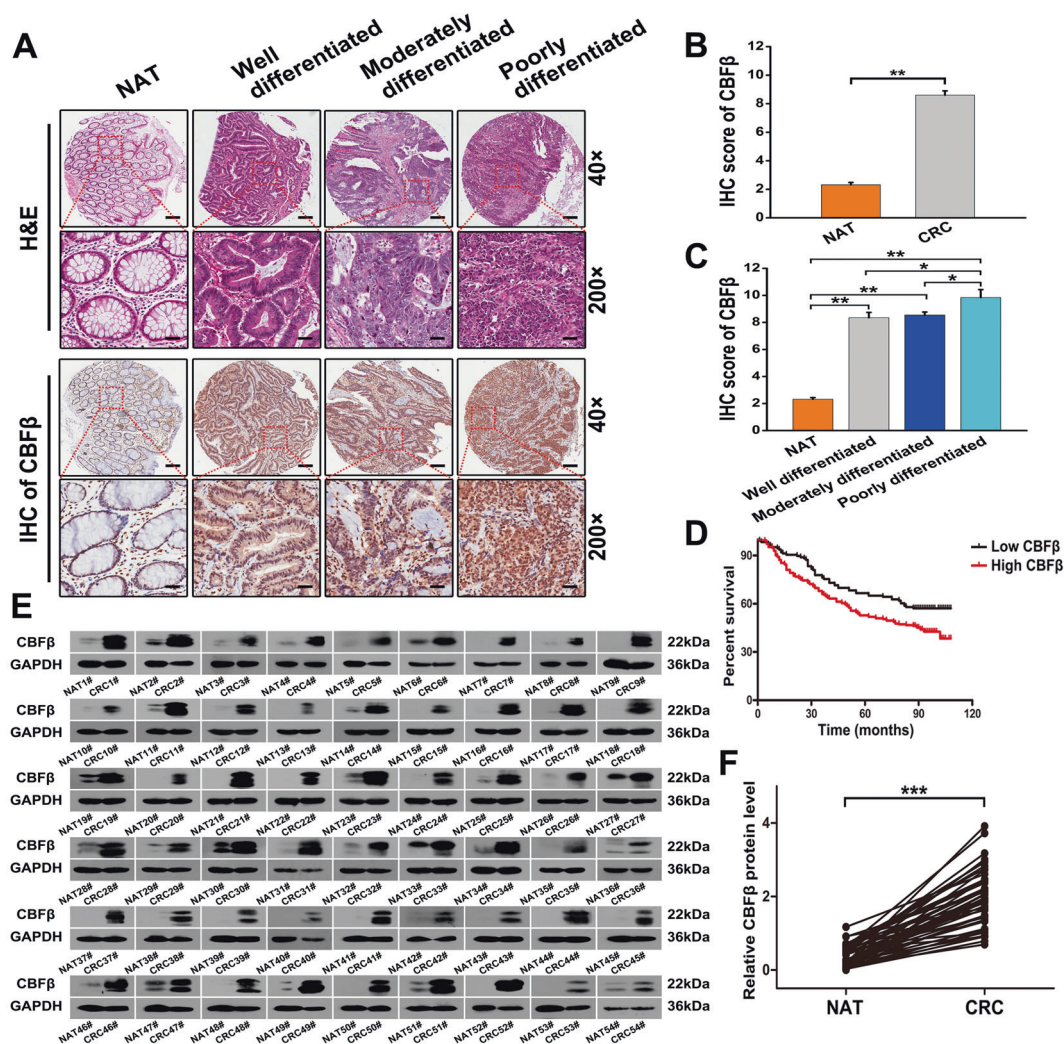
Fig. 1 Upregulation of CBFβ in colorectal cancer is associated with poor prognosis. A Representative photos of H&E staining and IHC staining of CBFβ protein in normal, well-differentiated, moderately differentiated, and poorly differentiated colorectal cancer tissues (magnification: ×40, scale bar = 250 μm; and magnification: ×200, scale bar = 50 μm). **B** Total IHC score of CBFβ in NAT and CRC tissues ($n = 180$, two-tailed Student's t test). **C** IHC score of CBFβ in normal, well-differentiated, moderately differentiated, and poorly differentiated colorectal cancer tissues (one-way ANOVA with post hoc Bonferroni correction). **D** Kaplan–Meier curves of overall survival of 180 patients with colorectal cancer, stratified by CBFβ expression. **E** Western blot analysis of CBFβ in NAT and CRC tissues ($n = 54$). GAPDH served as a loading control. **F** Quantification of the CBFβ protein bands compared to the GAPDH band from western blot of NAT and CRC tissues ($n = 54$), using ImageJ software for protein densitometric analysis (two-tailed Student's t test). Values are expressed as the mean ± SEM. *$P < 0.05$, **$P < 0.01$, ***$P < 0.001$.

Information). CCK-8 analysis showed that proliferation was increased in CBFβ-LV-HCT116 or CBFβ-LV-SW480 cells in a time-dependent manner, whereas cell proliferation was inhibited in shRNA-CBFβ-LV-HCT116 or shRNA-CBFβ-LV-SW480 cells compared with their control cells (Figs. 3A and S1C, Supporting Information). CBFβ overexpression markedly increased cell migration/invasion abilities and inhibited cell apoptosis in HCT116 and SW480 cells. Conversely, the potential for cell migration and invasion was suppressed, and the apoptosis rate and cleaved caspase-3/7 expression were elevated when endogenous CBFβ was inhibited (Figs. 3B–D and S1D–G, Supporting Information).

In addition, cell proliferation markers (Ki-67 and PCNA) were examined and CCK-8 assay was performed again after HCT116 cells were transfected with siRNAs against RUNX1-3 (for siRNA sequence, refer to Table S5, Supporting Information). The mRNA levels of Ki-67 and PCNA genes were reduced after RUNX2 was knocked down in cells (Fig. 3E). The upregulation of the Ki-67 and PCNA genes caused by CBFβ overexpression significantly decreased after cells were transfected with siRNA against RUNX2 rather than against RUNX1 or RUNX3 (Fig. 3F). The results of CCK-8 assay further confirmed that cell proliferation due to CBFβ overexpression was inhibited after cells were transfected with
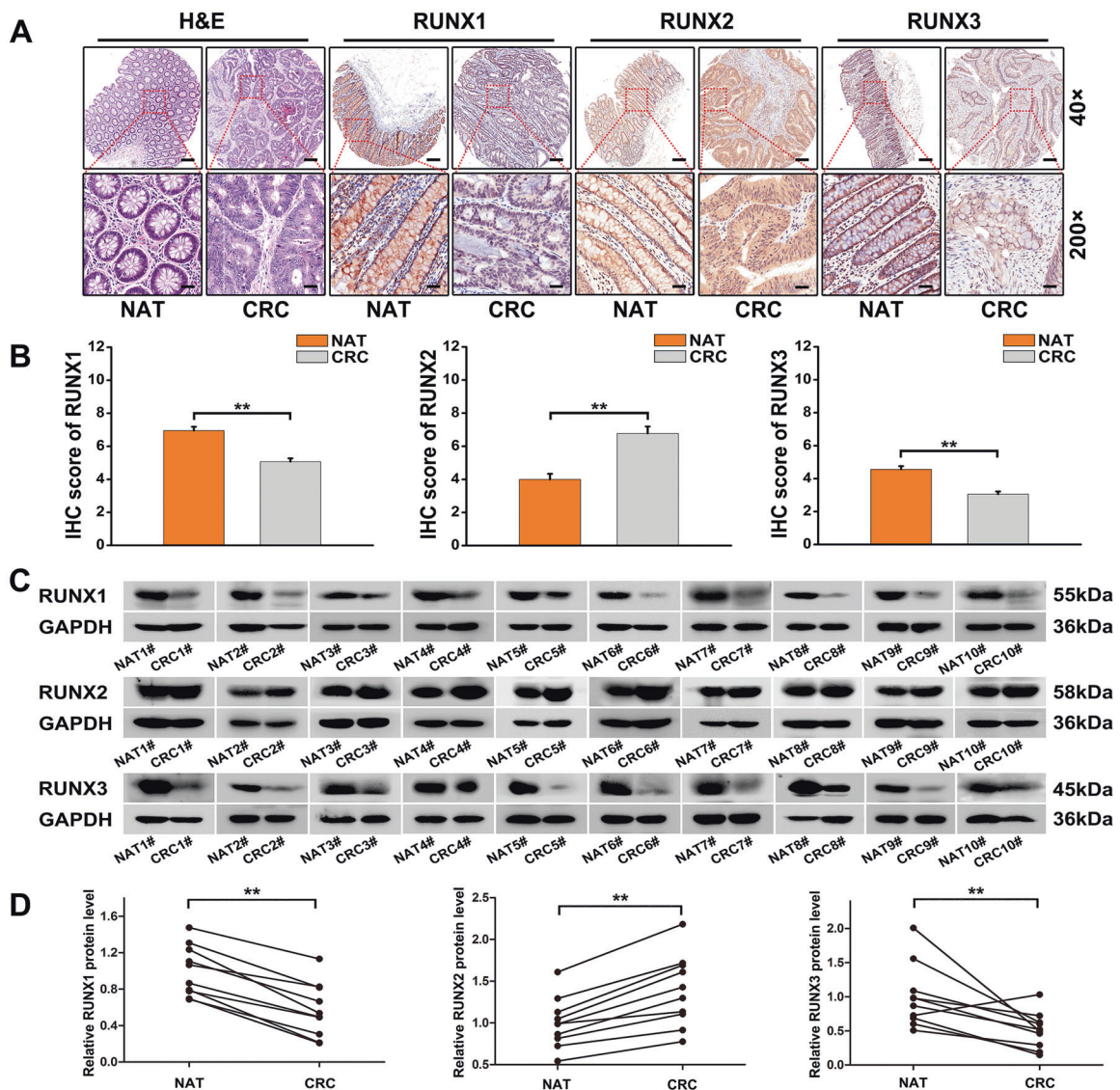
Fig. 2 RUNX1-3 expression in CRC patients. A Representative photos of H&E staining and IHC staining of RUNX1, RUNX2, and RUNX3 proteins in paired NAT and CRC tissues (magnification: ×40, scale bar = 250 μm; and magnification: ×200, scale bar = 50 μm). **B** Total IHC scores of RUNX1, RUNX2, and RUNX3 in NAT and CRC tissues (n = 75, two-tailed Student's t test). **C** Western blot analysis of RUNX1, RUNX2, and RUNX3 in NAT and CRC tissues (n = 10). GAPDH served as a loading control. **D** Quantification of the RUNX1, RUNX2, and RUNX3 protein bands compared to the GAPDH band from western blot in NAT and CRC tissues using ImageJ software for protein densitometric analysis (n = 10, two-tailed Student's t test). Values are expressed as the mean ± SEM. **P < 0.01.

siRUNX2 rather than siRUNX1 or siRUNX3, which suggested that the promoting effect of CBFβ on CRC cell proliferation might be RUNX2-dependent (Fig. 3G). The further results showed that the pro-metastatic and anti-apoptotic effects of CBFβ on CRC cells were abrogated when RUNX2 was inhibited (Figs. 3H–J and S2A, B, Supporting Information). Moreover, immunofluorescent staining demonstrated that the fluorescences of CBFβ and RUNX2 highly overlapped (Fig. 3K). Reciprocal co-IP experiments showed that endogenous RUNX2 and CBFβ interact in CRC cells (Fig. 3L). These results indicate that CBFβ promotes CRC cell proliferation, migration,

invasion, and inhibits CRC cell apoptosis in a RUNX2-dependent manner.

CBFβ-RUNX2 complex activates the transcription of OPN, FAM129A, and UPP1 in CRC cells

To identify genes that were transcriptionally affected by CBFβ, the cellular transcriptomes of stable HCT116 cells with CBFβ up/downregulation were analyzed, and the identified genes were subjected to functional clustering (Fig. S3A, Supporting Information). CBFβ upregulation resulted in 110 differentially expressed genes, and CBFβ
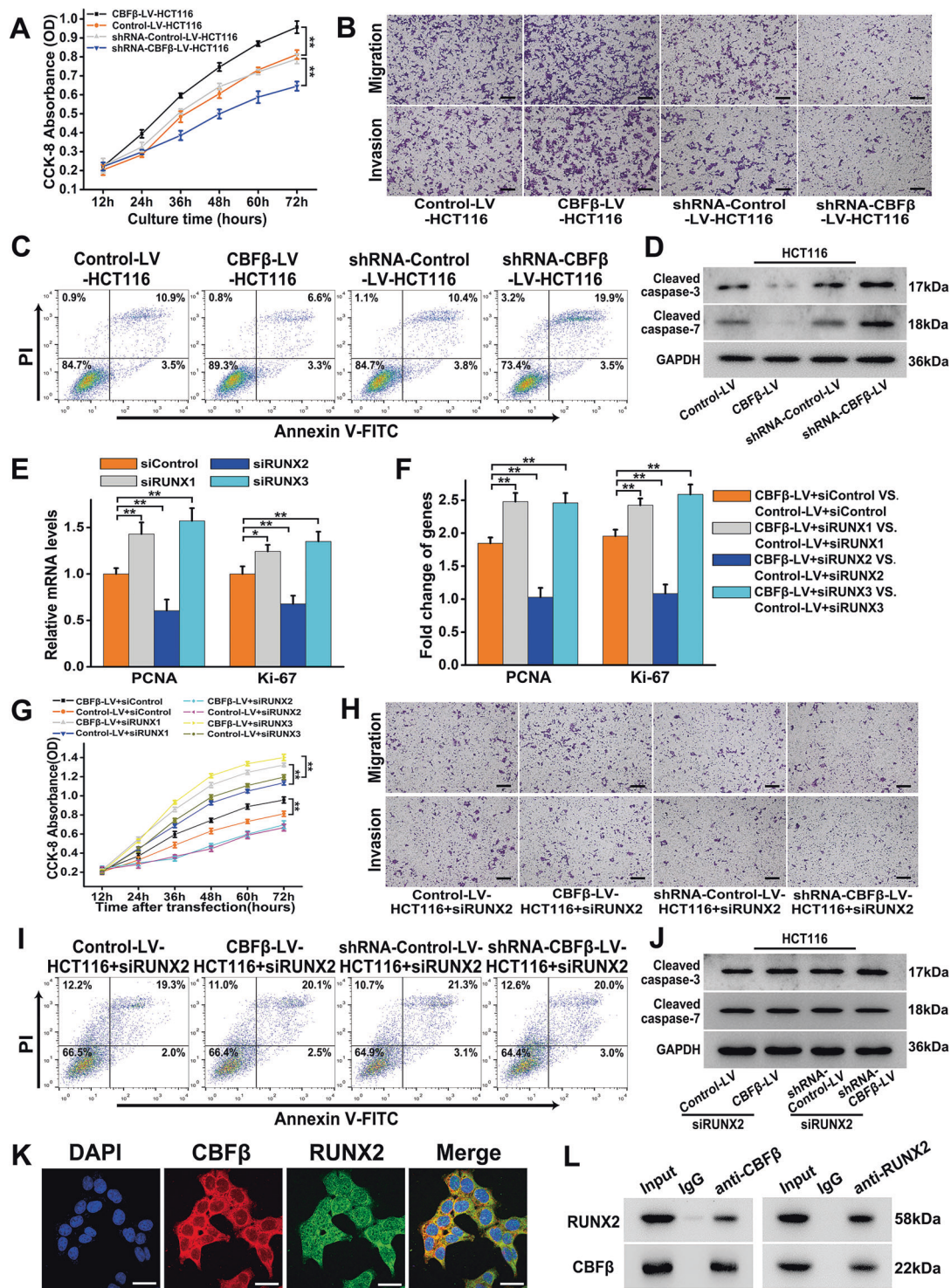
downregulation brought about 19 differentially expressed genes in HCT116 cells (fold change > 2, $p < 0.001$). Among the candidate genes with transcriptional differences, seven genes were observed in CBFβ upregulation/downregulation cells, as exhibited in the Venn diagram (Fig. 4A) and validated by quantitative real-time PCR (qRT-PCR) (Fig. S4, Supporting Information). Gene ontology (GO) and

KEGG pathway enrichment analysis indicated that the transcriptional responses mediated by CBFβ are mostly associated with cell proliferation, apoptosis, and metastasis, which was consistent with the results of the in vitro assays (Fig. S3B, Supporting Information). Taking into account that CBFβ does not possess DNA-binding activity and its pro-proliferation, pro-metastasis and anti-apoptosis

◄ **Fig. 3 CBFβ promotes CRC cell proliferation, migration, invasion, and inhibits CRC cell apoptosis in a RUNX2-dependent manner. A** Growth curves of stable HCT116 cells with overexpression or knockdown of CBFβ (CBFβ-LV/shRNA-CBFβ-LV groups) compared with their control cells (Control-LV/shRNA-Control-LV groups). Cell growth was measured using the CCK-8 assay ($n = 5$, two-tailed Student's *t* test). **B** Migration and invasion of CBFβ-LV/shRNA-CBFβ-LV-HCT116 cells and their control cells were examined by transwell assays after cells were plated and incubated for 12 h. One representative of three reproducible experiments is shown (scale bar = 100 μm). **C** Apoptosis of CBFβ-LV/shRNA-CBFβ-LV-HCT116 cells and their control cells was examined by flow cytometry. One representative of three reproducible experiments is shown. **D** Western blot analysis of cleaved caspase-3/7 protein in CBFβ-LV/shRNA-CBFβ-LV-HCT116 cells and their control cells. **E** Relative mRNA levels of PCNA and Ki-67 in HCT116 cells at 36 h after transfection with siRUNX1, siRUNX2, and siRUNX3 compared to the cells transfected with siControl (one-way ANOVA with the Dunnett's test). **F** Fold changes of mRNA levels of PCNA and Ki-67 in CBFβ-LV and Control-LV-HCT116 cells at 36 h after transfection with siRUNX1, siRUNX2, siRUNX3 or siControl (one-way ANOVA with the Dunnett's test). **G** Growth curves of CBFβ-LV and Control-LV-HCT116 cells after transfection with siRUNX1, siRUNX2, siRUNX3, or siControl. Cell growth was measured using the CCK-8 assay ($n = 5$, one-way ANOVA with post hoc Bonferroni correction). **H** Migration and invasion of CBFβ-LV/shRNA-CBFβ-LV-HCT116 cells and their control cells at 24 h post transfection with siRUNX2 were examined by transwell assays after transfected cells were plated and incubated for 12 h. One representative photo of three reproducible experiments is shown (scale bar = 100 μm). **I** Apoptosis of CBFβ-LV/shRNA-CBFβ-LV-HCT116 cells and their control cells at 36 h after transfection with siRUNX2 was examined by flow cytometry. One representative of three reproducible experiments is shown. **J** Western blot analysis of cleaved caspase-3/7 proteins in CBFβ-LV/shRNA-CBFβ-LV-HCT116 cells and their control cells at 36 h after transfection with siRUNX2. **K** Representative photos of immunofluorescence staining for CBFβ and RUNX2 (red, CBFβ; green, RUNX2; blue, DAPI nuclear staining). Pictures were imaged at ×40 magnification on a Nikon confocal microscope. Scale bar, 50 mm. **L** Coimmunoprecipitation of RUNX2 after pull down of the CBFβ protein complex (left) and coimmunoprecipitation of CBFβ after pull down of the RUNX2 protein complex (right) in HCT116 cells. One representative result of three experiments is shown. Values are expressed as the mean ± SEM. *$P < 0.05$; **$P < 0.01$.

functions are RUNX2-dependent, ChIP-seq analysis for RUNX2 was performed in order to further identify the downstream transcriptional targets of CBFβ/RUNX2 complex.

Through integrating RNA-seq data (7 CBFβ-dependent transcripts) with ChIP-seq data (RUNX2-bound genes), three candidate targets of the CBFβ-RUNX2 complex including OPN, FAM129A, and UPP1 were presented (Fig. 4B). The mRNA levels of OPN, FAM129A, and UPP1 genes increased 3.1-, 5.5-, and 2.6-fold, respectively, after overexpressing CBFβ (CBFβ-LV-HCT116 vs. Control-LV-HCT116) and decreased by about 50% after CBFβ was knocked down (shRNA-CBFβ-LV-HCT116 vs. shRNA-Control-LV-HCT116) (Fig. 4C). However, the effect of CBFβ alteration on OPN, FAM129A, and UPP1

mRNA expression was abrogated when inhibiting RUNX2 (Fig. 4D). Western blot results showed that the protein expression levels of OPN, FAM129A, and UPP1 were upregulated in CBFβ-LV-HCT116 cells and downregulated in shRNA-CBFβ-LV-HCT116 cells. RUNX2 interference caused markedly decreased protein levels of OPN, FAM129A, and UPP1 (Fig. 4E). The protein levels of OPN, FAM129A, and UPP1 obviously decreased in CBFβ-LV cells after transfected with siRUNX2 compared with CBFβ-LV cells transfected with siControl, demonstrating that CBFβ activates gene expressions of OPN, FAM129A, and UPP1 in a RUNX2-dependent way (Fig. 4F).

In addition, chromatin immunoprecipitation (ChIP) was performed to analyze the binding sites of the CBFβ-RUNX2 complex to the promoters of OPN, FAM129A, and UPP1. The ChIP-qPCR results demonstrated that different promoter regions of OPN (−183 to −20 and −2151 to −1735), FAM129A (−1588 to −906), and UPP1 (−417 to −238 and −2288 to −1864) were enriched by CBFβ and RUNX2 antibodies (Fig. 5A). To assess the activity that CBFβ-RUNX2 complex binds the promoters of OPN, FAM129A, and UPP1 in vitro, the CBFβ- and RUNX2-binding promoter fragments and their mutated fragments were subcloned into a pGL3-basic luciferase reporter plasmid. CBFβ significantly enhanced the luciferase activity of OPN, FAM129A, and UPP1 promoter plasmids (Fig. 5B). However, the increased luciferase activity mediated by CBFβ was abrogated by the luciferase reporter plasmids containing the mutated OPN, FAM129A, and UPP1 promoters (Fig. 5C). No change in luciferase activity was observed when altering CBFβ expression while simultaneously silencing RUNX2 (Fig. 5D). Together, these results showed that CBFβ could induce the transcriptional activation of OPN, FAM129A, and UPP1. This process is RUNX2-dependent.

CBFβ promotes colorectal tumor growth and liver metastasis in vivo

After nude mice were subcutaneously implanted with CBFβ-LV-HCT116, shRNA-CBFβ-LV-HCT116, or their control cells (7 mice/group), the tumor size in the CBFβ-LV-HCT116 group was significantly larger than that in the Control-LV-HCT116 group, whereas the tumor size in the shRNA-CBFβ-LV-HCT116 group had an opposite trend (Fig. 6A, B). The excised tumors from the CBFβ-LV-HCT116 group were 2.54-fold heavier than those from the Control-LV-HCT116 group, whereas the tumors from the shRNA-CBFβ-LV-HCT116 group weighed 53.2% less than those from the shRNA-Control-LV-HCT116 group at 30 days post implantation (Fig. 6C). The mRNA levels of the CBFβ-activated genes OPN, FAM129A, and UPP1 and
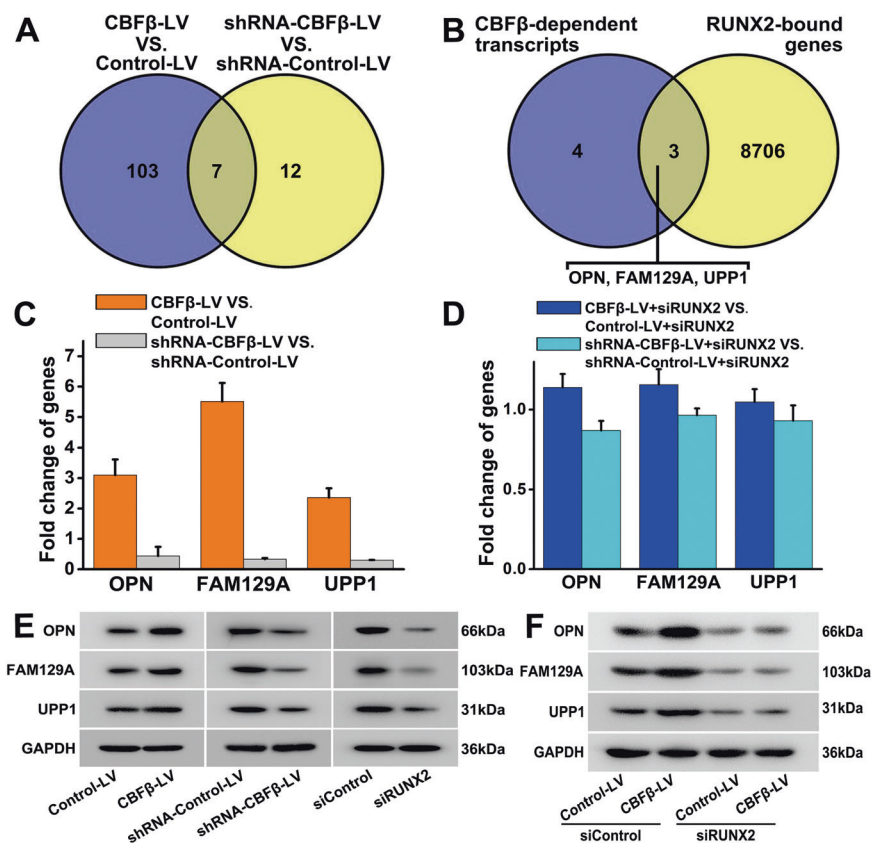
Fig. 4 CBFβ-RUNX2 complex promotes mRNA and protein expression of OPN, FAM129A, and UPP1 in CRC cells. A Intersection analysis of differently expressed genes both in CBFβ-LV-HCT116 and shRNA-CBFβ-LV-HCT116 cells. **B** Intersection analysis of CBFβ-dependent transcripts measured by RNA-seq and RUNX2-bound genes measured by ChIP-seq in HCT116 cells. **C** Fold changes of mRNA levels of OPN, FAM129A, and UPP1 in CBFβ-LV/shRNA-CBFβ-LV-HCT116 cells compared with their control cells (two-tailed Student's *t* test). **D** Fold changes of mRNA levels of OPN, FAM129A, and UPP1 in CBFβ-LV/shRNA-CBFβ-LV-HCT116 cells compared with their control cells after transfection with siRUNX2 for 36 h (two-tailed Student's *t* test). **E** Western blot analysis of OPN, FAM129A, and UPP1 protein in Control-LV, CBFβ-LV-HCT116 cells (left), shRNA-Control-LV, shRNA-CBFβ-LV-HCT116 cells (middle), and in HCT116 cells after transfection with siControl or siRUNX2 for 36 h (right). **F** Western blot analysis of OPN, FAM129A, and UPP1 proteins in CBFβ-LV and Control-LV-HCT116 cells after transfection with siControl or siRUNX2 for 36 h. Values are expressed as the mean ± SEM.

the proliferation and metastasis-associated genes PCNA, Ki-67, MMP-2, and MMP-9 were significantly increased in the tumors from CBFβ-LV-HCT116 group compared with those in the Control-LV-HCT116 group, whereas the mRNA levels of these genes in the shRNA-CBFβ-LV-HCT116 group had the opposite trend (Figs. 6D and S5A, B, Supporting Information). Western blot analysis and IHC staining for xenograft tumors also demonstrated that CBFβ markedly promoted OPN, FAM129A, UPP1, and Ki-67 expression, and inhibited cleaved caspase-3/7 expression (Figs. 6E and S5C, Supporting Information).

To evaluate the effect of CBFβ on CRC liver metastasis in vivo, CBFβ-LV-HCT116, shRNA-CBFβ-LV-HCT116, or their control cells were injected into the distal tip of the mouse spleen. Five weeks later, all of seven mice injected with CBFβ-LV-HCT116 cells formed liver metastases compared to four of seven mice injected with Control-LV-HCT116 cells.

In contrast, one of seven mice injected with shRNA-CBFβ-LV-HCT116 cells formed liver metastases, compared to four of seven mice injected with shRNA-Control-LV-HCT116 cells. In addition, livers and spleens of mice were harvested for histological examination (Figs. 6F and S6A, Supporting Information). The numbers of metastatic nodule in the liver from CBFβ-LV-HCT116 group (16 ± 1.86) significantly increased compared with those from Control-LV-HCT116 group (6 ± 1.40), whereas the numbers of metastatic nodule were much lower in the shRNA-CBFβ-LV-HCT116 group (2 ± 0.63) than those in the shRNA-Control-LV-HCT116 group (5 ± 1.52). IHC analysis of metastatic nodule in the liver also demonstrated that CBFβ markedly enhanced Ki-67 expression and suppressed cleaved caspase-3/7 expression (Fig. S6B, Supporting Information). These findings indicated that CBFβ could promote CRC growth and liver metastasis in vivo.
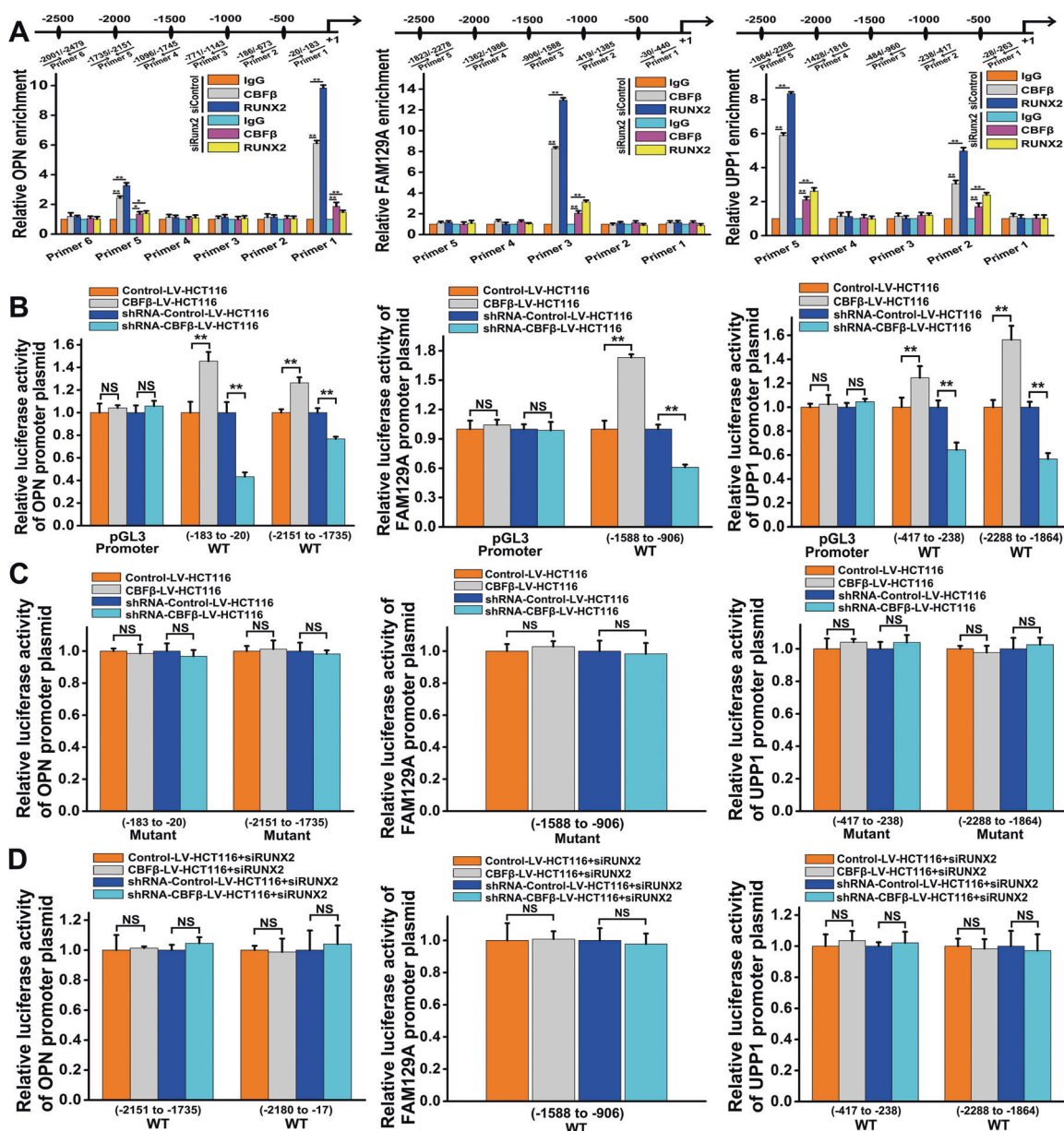
Fig. 5 Binding sites of CBFβ-RUNX2 complex in the promoter regions of OPN, FAM129A, and UPP1 were identified in CRC cells. A The enrichment of OPN, FAM129A, and UPP1 promoter fragments precipitated by CBFβ or RUNX2 antibody, which was demonstrated by chromatin immunoprecipitation (ChIP) analysis. Further experiments were performed when simultaneously inhibiting RUNX2. Rabbit IgG served as a control (one-way ANOVA with post hoc Bonferroni correction). **B** The parental pGL3 reporter and the modified pGL3 reporters containing the predicted binding sites of RUNX2 on the promoters of OPN, FAM129A, and UPP1 were transfected in CBFβ-LV/shRNA-CBFβ-LV-HCT116 cells and their control cells. After 24 h, the reporter activity was measured using a luciferase assay. **C** The reporter activity was measured after transfection with the plasmids, in which the predicted binding sites of RUNX2 on the promoters of OPN, FAM129A, and UPP1 were mutated. **D** The reporter activity was measured after cotransfection with siRNA for RUNX2 and modified pGL3 reporters containing the predicted binding sites of RUNX2 on the promoters of OPN, FAM129A, and UPP1 simultaneously (**B–D**: two-tailed Student's t test). Values are expressed as the mean ± SEM. $*P < 0.05$; $**P < 0.01$; NS, no significance.

CBFβ is targeted by miR-143 and miR-145 in CRC

As shown in Fig. 7A, a 1.99-fold increase of CBFβ mRNA level was found in 54 CRC tissues compared with the NAT; however, significantly upregulated CBFβ protein levels in CRC tissues suggested that posttranscriptional regulation, such as miRNA regulation, is probably involved in CBFβ overexpression (Fig. 1A, E). Four bioinformatics prediction methods, including TargetScan, miRanda, PITA, and RNAhybrid, revealed miR-143 and miR-145 as probable candidates to regulate CBFβ expression. The predicted interactions between miR-143/145 and the targeting sites
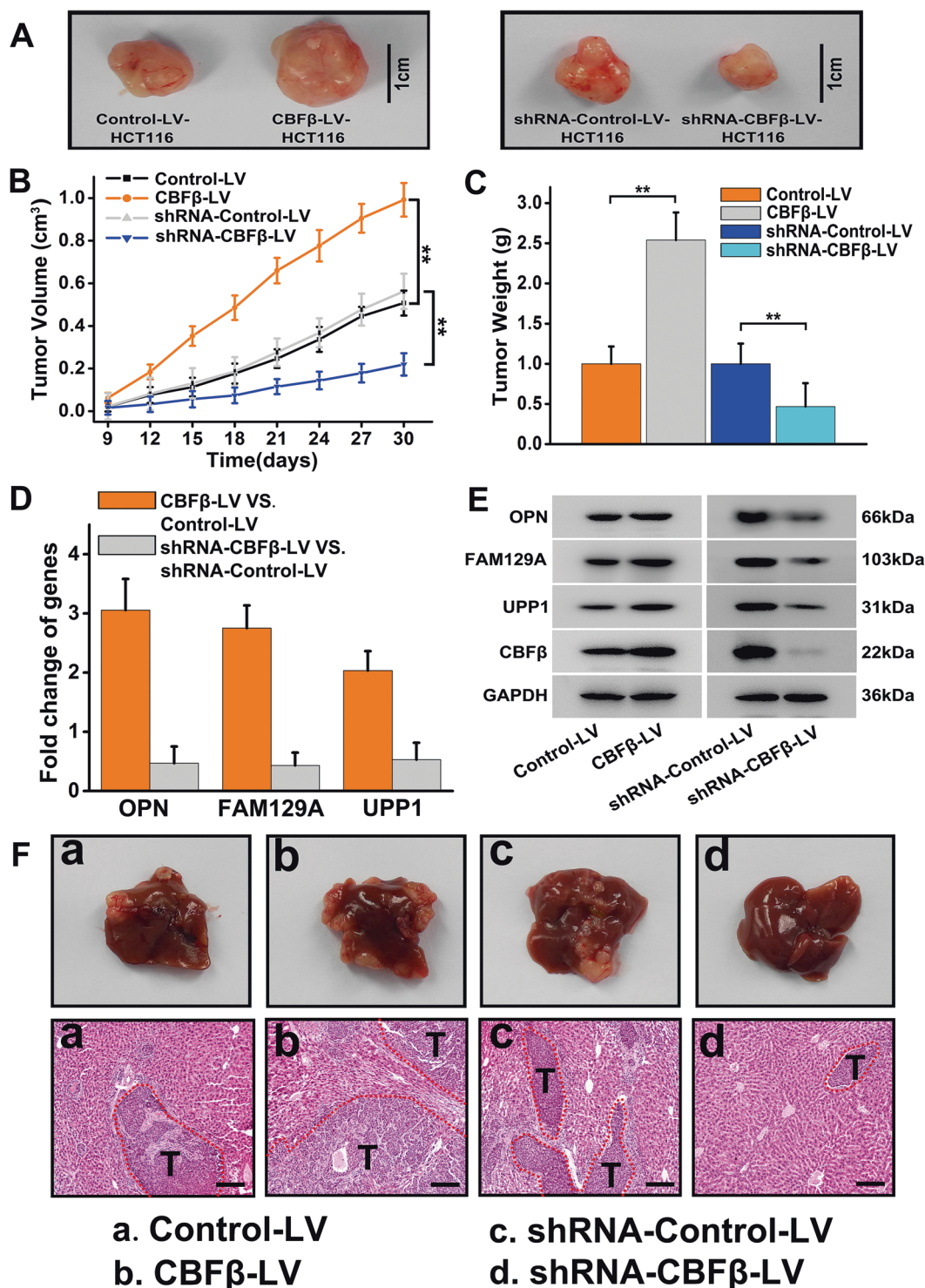
Fig. 6 CBFβ promotes colorectal tumor growth and liver metastasis in vivo. A Representative photographs of xenograft tumors derived from nude mice with subcutaneous implantation of CBFβ-LV/shRNA-CBFβ-LV-HCT116 cells or their control cells. The volumes (left) and weights (right) of the xenograft tumors derived from nude mice with subcutaneous implantation of CBFβ-LV/shRNA-CBFβ-LV-HCT116 cells or their control cells (**B, C**: two-tailed Student's *t* test). **D** Fold changes of mRNA levels of OPN, FAM129A, and UPP1 in xenograft tumors from nude mice (two-tailed Student's *t* test). **E** Western blot analysis of OPN, FAM129A, UPP1, and CBFβ proteins in xenograft tumors from nude mice. **F** Representative photographs and H&E staining images of livers derived from nude mice with spleen injection of CBFβ-LV/shRNA-CBFβ-LV-HCT116 cells or their control cells. T tumor region. One representative result of three experiments is shown (scale bar = 100 μm). Values are expressed as the mean ± SEM. **$P < 0.01$.
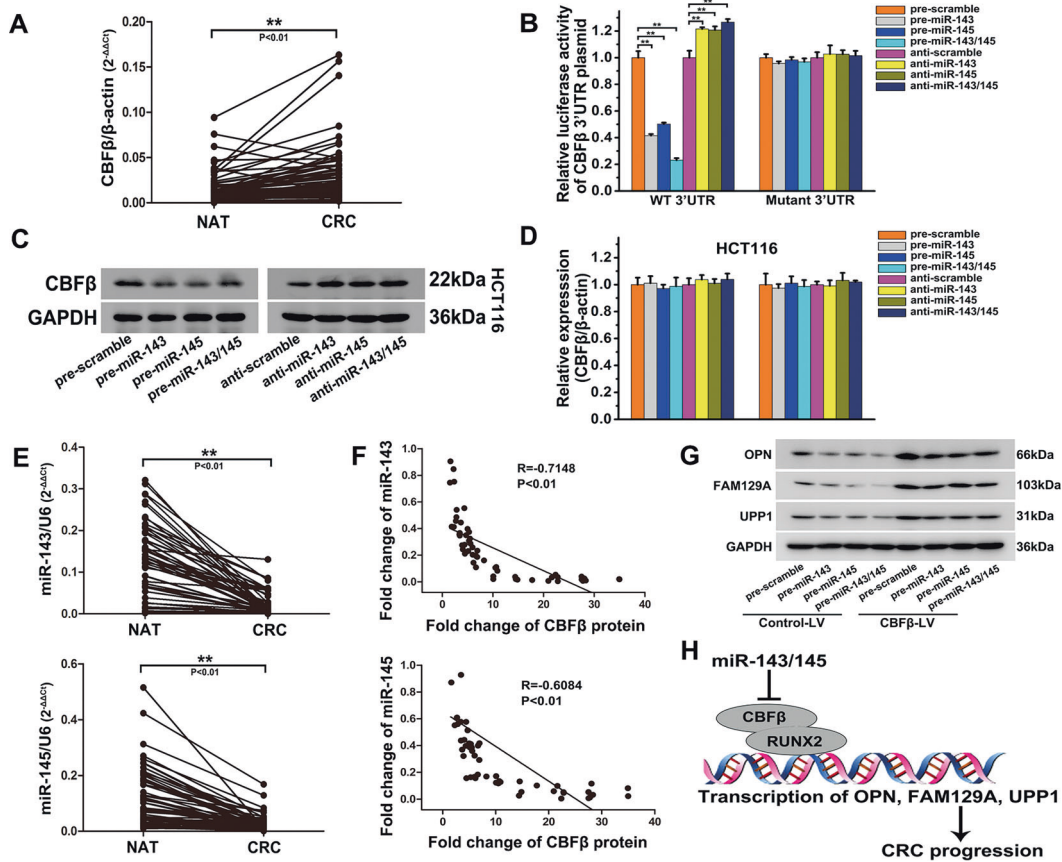
Fig. 7 MiR-143 and miR-145 directly regulate CBFβ expression at the posttranscriptional level in CRC. A qRT-PCR analysis of CBFβ mRNA level in 54 pairs of CRC and NAT samples (two-tailed Student's t test). **B** Direct recognition of the CBFβ 3′-UTR by miR-143/145. HCT116 cells were cotransfected with firefly luciferase reporters containing either wild-type (WT) or mutant miR-143/145 binding sites in the CBFβ 3′-UTR and pre-scramble, pre-miR-143, pre-miR-145, pool of pre-miR-143 and pre-miR-145, anti-scramble, anti-miR-143, anti-miR-145, or pool of anti-miR-143 and anti-miR-145. The cells were evaluated using a luciferase assay kit after 24 h. The results are displayed as the ratio of firefly luciferase activity in the miR-143/145-transfected cells compared to the activity in the control cells (one-way ANOVA with the Dunnett's test). **C** Western blot analysis of CBFβ protein level and **D** qRT-PCR analysis of relative CBFβ mRNA level in HCT116 cells treated with pre-scramble, pre-miR-143, pre-miR-145, or pool of pre-miR-143 and pre-miR-145, and in cells treated with anti-scramble, anti-miR-143, anti-miR-145, or pool of anti-miR-143 and anti-miR-145. **E** qRT-PCR analysis of the expression levels of miR-143 (up) and miR-145 (down) in NAT and CRC tissues ($n = 54$) shown as line charts. U6 small nuclear RNA was used as an internal control to normalize expression data (two-tailed Student's t test). **F** Pearson's correlation scatter plot showing the fold changes in expression of CBFβ protein and miR-143 (up) or miR-145 (down) in CRC patients ($n = 54$). The correlation coefficient (R) is shown. **G** The protein levels of OPN, FAM129A, and UPP1 in CBFβ-LV-HCT116 and Control-LV-HCT116 cells after transfection with pre-scramble, pre-miR-143, pre-miR-145, or pool of pre-miR-143 and pre-miR-145. **H** Schematic diagram of miR-143/145-targeted CBFβ to promote CRC progression through transcriptionally activating OPN, FAM129A, and UPP1 in a RUNX2-dependent manner. Values are expressed as the mean ± SEM. **$P < 0.01$.

within the 3′-untranslated region (3′-UTR) of CBFβ are illustrated (Fig. S7, Supporting Information). As shown in Figs. 7B and S8A (Supporting Information), overexpression of miR-143 or miR-145 exerted repressive effects on 3′-UTR (CBFβ) reporter expression with a 58.4 or 53.9% reduction in luciferase reporter activity in HCT116 and SW480 cells. Inhibition of miR-143 or miR-145 resulted in a 21.6 or 20.7% increase in reporter activity compared with the controls. The mutation of miR-143 and miR-145 binding sites abolished the above effects. Compared with the control, the overexpression of miR-143,

miR-145, and miR-143/145 resulted in a significant decrease in CBFβ protein level, whereas their inhibition led to an increase of CBFβ protein level in HCT116 and SW480 cells (Figs. 7C and S8B, Supporting Information). However, unlike the variation in CBFβ protein level, the CBFβ mRNA level was not significantly changed by the overexpression or inhibition of miR-143/145 (Figs. 7D and S8C, Supporting Information). In addition, the levels of miR-143 and miR-145 were found to be significantly downregulated in 54 CRC tissues compared with NAT using qRT-PCR (Fig. 7E). A significant inverse correlation

was exhibited between fold changes of miR-143 or miR-145 and fold change of CBFβ protein in CRC patients, as indicated by Pearson correlation (Fig. 7F). These results suggested that miR-143/145 regulated CBFβ expression probably via a translational repression mechanism rather than by affecting its mRNA stability.

Thereafter, the downstream mechanism of miR-143/miR-145 targeting CBFβ was studied in CBFβ-overexpressing cells or its control cells (Fig. 7G). The protein levels of OPN, FAM129A, and UPP1 were obviously reduced in Control-LV-HCT116 cells after transfection with pre-miR-143/pre-miR-145. The suppression effects of pre-miR-143/pre-miR-145 on OPN, FAM129A, and UPP1 were greatly rescued in CBFβ-overexpressing cells. Together, these data indicated that miR-143/miR-145 targeted CBFβ and could downregulate the expression of OPN, FAM129A, and UPP1 in CRC cells (Fig. 7H).

Discussion

As a non-DNA-binding protein, CBFβ often dimerizes with RUNXs with the help of their RUNT domain, enhancing the binding and recognition of the consensus sequence PyG-PyGGTPy of target genes [25]. CBFβ may exert distinct functions when binding with different RUNX members. For instance, RUNX1 works together with CBFβ-SMMHC to regulate critical genes in abnormal myeloid progenitors for leukemia development [26]. CBFβ interacts with RUNX1 and RUNX2 to maintain the metastatic phenotype of breast cancer cells [9, 27]. CBFβ-RUNX3 complex antagonizes CCL5's enhancer and mediates its repression, which modulates antitumor immunity in mouse melanoma models [28]. However, which RUNX works with CBFβ to affect CRC progression is poorly understood. In this study, among the three RUNXs, only RUNX2 was found to be upregulated in human CRC tissues compared with non-tumor tissues, which is necessary for CBFβ to affect CRC cells. It is noteworthy that the expression level of RUNX2 in non-tumor tissues is high (Fig. 2A, D), which points to its importance for physiology of the colon. RUNX2 is reported to be an important factor involved in the transcription of BMP target genes, which contributes to the regulation of intestinal stem cell self-renewal [29, 30]. These results suggest that RUNX2 plays a key role in maintaining crypt homeostasis. However, the action of CBFβ-RUNX2 complex and their downstream effectors in CRC remain unclear.

In the present study, OPN, FAM129A, and UPP1 were found to be transcriptionally activated by CBFβ-RUNX2. OPN was upregulated in CRC patients and associated with higher tumor stage and poor prognosis [31]. Following the binding to $\alpha_v\beta$ integrin and CD44 receptors, OPN affects the proliferation, metastasis, and apoptosis signals [32], which coincided with our GO and KEGG results (Fig. S3B, Supporting Information). OPN knockdown suppresses CRC cell proliferation, cell invasion, and murine liver metastasis [33], and OPN deficiency inhibits intestinal tumorigenesis in Apc^{Min} mice [34]. FAM129A (also named Niban, C1orf24) is overexpressed in CRC [35], and the down-regulation of FAM129A mediated by ZNF777 inhibits CRC cell proliferation [36]. Ubiquitously expressed UPP1 catalyzes the reversible phosphorolysis of uridine to uracil, and serves as the main enzyme involved in uridine homeostasis and pyrimidine salvage [37]. In normal colonic epithelium, vitamin-D-caused UPP1 upregulation leads to low-uridine-induced DNA damage [38]. During CRC development, UPase overexpression associates with tumor stages [39], and UPP1 mRNA levels were higher in metastatic liver than in primary tumors [40]. UPP1 overexpression might provide a formidable support for uridine metabolism and nucleic acid synthesis in CRC cells. Taken together, these findings suggest that OPN, FAM129A, and UPP1 have oncogenic effects in CRC progression. In this study, an ascending trend of OPN, FAM129A, and UPP1 mRNA expressions was found in CRC patients, and OPN had a higher expression level and fold change (Fig. S9, Supporting Information), highlighting these three genes, especially OPN, are responsible for CBFβ-RUNX2-mediated oncogenic effects.

Compared with the minor fold change of CBFβ mRNA in CRC patient (Fig. 7A), significantly upregulated CBFβ protein was found in tumor tissues of CRC patient (Fig. 1A, E), suggesting that posttranscriptional regulation, such as miRNA regulation, is probably involved in CBFβ over-expression. In this study, TargetScan, miRanda, PITA, and RNAhybrid were combined to predict 13 miRNAs that potentially regulate CBFβ (Table S6, Supporting Information). Among the 13 miRNAs, the six miRNAs (miR-223, miR-483-3p, miR-300, miR-877, miR-200a, miR-19b) were reported to be upregulated in CRC [41–46]. Therefore, these six miRNAs can not regulate CBFβ due to its over-expression in CRC patients. Other seven miRNAs (miR-1303, miR-940, miR-539, miR-217, miR-424, miR-143, miR-145) were found to be downregulated in CRC patients (Figs. 7E and S10A, Supporting Information). Particularly, out of the seven miRNAs that were downregulated, miR-143 and miR-145 have higher expression levels in clinical NAT and CRC tissues than the other five miRNAs according to qRT-PCR results (Figs. 7E and S10B, Supporting Information). MiR-143 or miR-145 were confirmed to exert more considerable suppression on the luciferase activity of the CBFβ 3'-UTR reporter (Fig. S10C, Supporting Information). Moreover, a significant inverse correlation between the expressions of

decreased miR-143/miR-145 and upregulated CBFβ protein was found in CRC patients, therefore, we considered that miR-143 and miR-145 might act as dominant tumor-suppressive miRNAs to regulate CBFβ expression in CRC. In addition to miR-143 and miR-145, miR-125b has been reported to be activated by transcription factor CDX2, which in turn inhibits CBFβ translation, thereby counter-acting myeloid cell differentiation in hematopoietic malignancies [47]. However, miR-125b was found to be upregulated in CRC, indicating that miR-125b could not regulate CBFβ in CRC [48]. Taken together, these results demonstrate that miRNA regulation provide a compelling explanation for CBFβ expression dysregulation in CRC.

In conclusion, our findings demonstrate that CBFβ promotes CRC progression through activating tumorigenic gene expression of OPN, FAM129A, and UPP1 in a RUNX2-dependent manner and identifies a miR-143/145-mediated mechanism in modulating CBFβ expression. Thus, the regulatory signals might provide prognostic and therapeutic potential for the treatment of CRC.

Materials and methods

Clinical samples and cell lines

Two TMAs consist of clinical CRC tissues, obtained from Shanghai Outdo Biotech (Shanghai, China). One TMA containing 180 CRC tissues and matched NAT with 9-year follow-up data was used for CBFβ analysis by IHC (Table S1, Supporting Information). Another TMA with 75 pairs of CRC tissues and NAT samples was used for IHC analysis of RUNX1, RUNX2, and RUNX3 (Table S2, Supporting Information). In addition, 54 paired tumor tissues and NAT were obtained from CRC patients who underwent radical resection at Jinling Hospital (Nanjing, China) and were used for CBFβ analysis by western blot (Table S3, Supporting Information). All patients have signed the informed consent form. The study protocol was approved by the Medical Ethics Committee of the Affiliated Jinling Hospital of Nanjing University (2018NLY-046) and complied with the principles described in the WMA Declaration of Helsinki and the Department of Health and Human Services Belmont Report.

Human colorectal carcinoma HCT116 and colorectal adenocarcinoma SW480 cells were obtained from the Institute of Cell Biology at the Chinese Academy of Sciences (Shanghai, China) and cultured in RPMI 1640 medium (Invitrogen, Camarillo, CA, USA) containing 10% FBS (Invitrogen). Cells were authenticated in 2018 by STR profiling, and routinely checked for mycoplasma contamination by PCR.

Histology and IHC analysis

As previously described [49], hematoxylin and eosin (H&E) staining was performed using 5-μm-thick paraffin-embedded sections of human or mouse CRC tissues. For immunohistochemical analysis, the deparaffinized sections underwent antigen retrieval at 95 °C for 20 min in citrate solution (pH 6) and incubation of H_2O_2 (0.3%) for 30 min to block the endogenous peroxidase activity. Sections were then subjected to 3% BSA blocking and incubated with primary antibodies against CBFβ, RUNX1-3, Ki-67, cleaved caspase-3, or cleaved caspase-7 overnight at 4 °C, followed by excessive washing and incubation of biotinylated anti-rabbit or anti-mouse secondary antibody (Vector Laboratories, Burlingame, CA, USA) for 60 min at room temperature. Specific labeling was detected using diaminobenzidine (Vector Laboratories) as the chromogen. The sections were counterstained with hematoxylin to label nuclei, dehydrated in graded concentrations of ethanol and mounted.

IHC staining images were scored using the semi-quantitative immunoreactive score (IRS) system by two experienced pathologists in a blinded manner. The intensity of immunostaining was given a score of 0–3 (0, negative; 1, weak; 2, moderate; 3, strong), and the cell percentage with positive staining cells was given a score of 1–4 (1, 0–25%; 2, 26–50%; 3, 51–75%; and 4, 76–100%). Multiplication of the intensity and the percentage of marker-positive cells resulted in an IRS ranging from 0 to 12 for each sample. Samples with IRS < 8 were classified as the CBFβ low expression group, and those with IRS ≥ 8 were defined as the CBFβ high expression group. Based on the follow-up data of 180 CRC patients 9 years after diagnosis, the overall survival curve depending on CBFβ expression was determined using the Kaplan–Meier method.

Western blot analysis

Protein extracts of cells and tissues were prepared using RIPA lysis buffer with freshly added protease inhibitor cocktail (Sigma-Aldrich, St. Louis, MO, USA), and total protein content was quantified by the BCA protein assay kit (Thermo Scientific, Rockford, IL, USA). Then, protein was separated by SDS-PAGE gel and transferred onto a polyvinylidene fluoride membrane (Millipore, Bedford, USA). Membranes were blocked with 5% nonfat milk and incubated with primary antibodies followed by the HRP-conjugated secondary antibody (Jackson ImmunoResearch Laboratories, West Grove, PA, USA). Signals were visualized using an ECL detection reagent (Thermo Scientific). GAPDH was used as loading control. The information of antibodies used in this study is listed in Table S7 (Supporting Information).

Establishment of stable cell lines and siRNA transfection

Full-length human CBFβ was cloned into the lentiviral expression vector pLVX-puro (Addgene, Cambridge, MA, USA) by GeneCopoeia (Guangzhou, China). CBFβ-expressing lentivirus (CBFβ-LV) and control lentivirus (Control-LV) were generated as described previously [49]. In addition, lentiviral constructs of CBFβ shRNA or the scramble control (GeneCopoeia, Table S5, Supporting Information) were introduced into HEK293 cells to produce CBFβ-downregulating lentivirus (shCBFβ-LV) or control lentivirus (shControl-LV). After infection with CBFβ-LV, Control-LV, shCBFβ-LV, or shControl-LV, stable HCT116 and SW480 cells were established by antibiotics selection, and CBFβ levels in the stable transfectants were analyzed by qRT-PCR and western blot analysis to validate overexpression or knockdown efficiency of CBFβ.

To silence RUNX expression, siRNAs targeting RUNX1, RUNX2, and RUNX3 were synthesized (Life Technologies, Shanghai, China), and the most effective siRNAs against RUNX1-3 were used in the in vitro experiments (Table S5, Supporting Information). Transfection assays were carried out using the Lipofectamine 2000 reagent (Invitrogen) according to the manufacturer's instructions.

Cell proliferation assay

Cell proliferation assay was performed using the Cell Counting Kit-8 (CCK-8) assay (Dojindo, Kumamoto, Japan). Briefly, cells were seeded onto 96-well plates at a density of 5000 cells per well. Cells were then treated with the indicated reagents and evaluated after incubation for 12, 24, 36, 48, 60, and 72 h. Triplicate measurements were performed at each time point.

Cell migration and invasion analysis

For cell migration analysis, cells were plated on six-well plates, and linear scrape wounds were made on the cell monolayer when grown to confluence. Cells were washed with PBS and then cultured in medium with serum. The wound closure was imaged under a microscope immediately after wound creation at 0, 6, 24 h post scratch. The distances from the edge to the middle of the scratch were determined using imageJ software (http://rsb.info.nih.gov/ij/) to quantify the wound percentage.

For cell invasion analysis, 1×10^5 cells were plated into the top chamber of the insert (Corning Costar) for the cell migration assay, or 2×10^5 cells were plated in the top chamber precoated with 1-mg/ml Matrigel (BD Bioscience, San Jose, CA, USA) for the cell invasion assay. Then, cells were cultured in the top chamber with serum-free medium, and medium supplemented with 10% FBS was used as a chemoattractant in the lower chamber. After 12 h, non-motile cells at the top of the filter were removed, and the cells that migrated to the underside of the membrane were fixed with methanol, stained with crystal violet, and imaged.

Flow cytometry analysis

Cells were harvested and washed three times with cold PBS, then added into 500-μL binding buffer containing 5-μL Annexin V-FITC and 10-μL PI at room temperature for 15 min. Surface exposure of phosphatidylserine in apoptotic cells was measured by an Annexin V/PI apoptosis detection kit according to the manufacturer's instructions (BD Biosciences, Franklin Lakes, NJ, USA), then the cells were then analyzed with an Attune NxT flow cytometer (Invitrogen). The cell apoptosis percentage was analyzed using a FlowJo software (TreeStar, Ashland, OR, USA).

qRT-PCR assay

Total RNA from cultured cells and patient tissues was prepared using TRIzol reagent (Invitrogen). qRT-PCR assays were performed using the One Step SYBR PrimeScript RT-PCR Kit (Takara, Shiga, Japan) to analyze gene expression or using the SYBR PrimeScript miRNA RT-PCR Kit (Takara) to examine miRNA levels. β-actin served as an internal control for gene expression, and U6 snRNA was used as the miRNA internal control. The primer sequences for qRT-PCR are listed in Table S8 (Supporting Information).

Immunofluorescence and immunoprecipitation assays

For immunofluorescence studies, HCT116 cells were plated on poly-D-lysine-coated glass slides, fixed in 4% paraformaldehyde and permeabilized with 0.1% Triton X-100. Nonspecific binding was prevented by incubation with 5% BSA for 1 h. Staining was carried out by incubating cells with anti-CBFβ and anti-RUNX2 antibodies overnight. The corresponding TRITC-labeled rabbit anti-goat secondary antibody and FITC-labeled goat anti-mouse/rat antibody were applied at room temperature for 1 h, and then nuclear DAPI staining was performed. All fluorescence images were captured on a Nikon confocal microscope (C2+, Nikon, Tokyo, Japan). All immunofluorescence staining experiments and in situ hybridizations were repeated in triplicate with multiple serial sections, including negative controls, to determine the background staining.

For immunoprecipitation studies, 1-mg cell lysates were incubated with 1-μg antibodies and further incubated with protein A/G sepharose beads (Merck Millipore) for 4 h. Then, the immunoprecipitate was eluted with a sample

buffer (1% SDS, 100-mM DTT, 50-mM Tris, pH 7.5). Immunoprecipitation was performed using anti-CBFβ, anti-RUNX2 antibodies, or rabbit/mouse normal IgG, followed by western blot analysis.

Transcriptome sequencing analysis and ChIP-seq analysis

For transcriptome sequencing analysis, total RNA was extracted from HCT116 cells stably expressing or inhibiting CBFβ (CBFβ-LV/shRNA-CBFβ-LV groups) or their control cells (Control-LV/shRNA-Control-LV groups) using TRIzol (Life Technologies). RNA extraction was performed in triplicate and pooled to one sample for each group of cells. Total RNA was treated with RNase-free DNase I (New England Biolabs, MA, USA) to remove any contaminating genomic DNA. mRNA extraction was performed using Dynabeads oligo (dT) (Invitrogen). Double-stranded complementary DNAs were synthesized using Superscript II reverse transcriptase (Invitrogen) and random hexamer primers. RNA was subjected to fragmentation and library construction and then sequenced with the HiSeq 2000 platform. For the data analysis, base calls are performed using CASAVA. Sequencing tags were aligned to the human genome using TopHat. Cufflinks were used to calculate the fragments per kilobase of transcript sequence per million base pairs sequenced (FPKM). Differentially expressed genes with a p value of 0.005 or less and an absolute fold change of 2 or more were clustered and visualized using a clustergram heatmap. For enrichment analysis of GO and Kyoto Encyclopedia of Genes and Genomes (KEGG), the differentially expressed gene lists were analyzed in the Database for Annotation, Visualization, and Integrated Discovery annotation tools [http://david.abcc.ncifcrf.gov/] and selected based on $p < 0.01$. All of the procedures were carried out by Novogene (Beijing, China) according to Illumina's protocols.

ChIP assay was performed using a ChIP assay kit (Millipore, Temecula, USA) according to the manufacturer's instructions. Cells were fixed with formaldehyde and homogenized. Nuclei were pelleted, and DNA was sheared by sonication and immunoprecipitated with anti-CBFβ antibody, anti-RUNX2 antibody, or negative control immunoglobulin G using protein A/G beads. DNA was released from immunoprecipitate complexes using proteinase K and purified. Chromatin was sheered by eight sonication cycles to generate DNA fragments with an average size of 200 bp for ChIP-seq analysis and four sonication cycles to generate DNA fragments with an average size of 600 bp for ChIP-qPCR.

For high-throughput sequencing, DNA (10–20 ng) was used to make the ChIP-seq library according to the instructions from Illumina's ChIP-seq Sample Prep kit. The

ChIP-seq library was loaded on Illumina's cluster station and sequenced with Illumina Genome Analyzer IIx. Sequenced reads of ChIP-seq analysis were aligned to the human genome, and reads with more than two aligned positions were removed. The remaining tags were further filtered by quality score and redundancy. Only non-redundant reads that passed the quality score were retained for downstream analysis. ChIP-seq tags and whole-genome sequencing tags were then analyzed using MACS to identify the peaks based on $p < 0.005$ [50]. The data of transcriptome sequencing and ChIP-seq have been deposited in NCBI Gene Expression Omnibus (GEO accession number GSE154876).

Equal amounts of sonicated HCT116 chromatin DNA were incubated with IgG control, CBFβ, or RUNX2 antibody. Protein G bead-captured chromatin DNA was amplified as a template, and different pairs of primers across the promoters of OPN, FAM129A, and UPP1 were used for quantitative real-time PCR. A standard curve was prepared for each set of primers using serial titration of the input DNA. ChIP-DNA was analyzed by qPCR, and the enrichment was expressed as the percentage of the input DNA from primer-specific standard curves using Rotor-Gene 6000 Series Software 1.7. The corresponding primers are listed in Table S9 (Supporting Information).

Plasmid constructs and luciferase reporter assay

For the promoter luciferase assay, different promoter fragments containing RUNX2-binding sites of the OPN, FAM129A, and UPP1 genes, which were predicted by JASPAR, were amplified by PCR using a human genomic DNA template made from HCT116 cells and were subsequently cloned into the pGL3-basic luciferase reporter plasmid (Promega, Madison, WI, USA). Efficient insertion was confirmed by sequencing. To evaluate promoter activities, the constructed reporters with different promoter regions were transfected into CBFβ-LV-HCT116 and shRNA-CBFβ-LV-HCT116 cells and the corresponding controls. The binding site mutants (OPN binding site 1 within −183 to −20, CCAGATTGTGGTCTG replaced by GTCTGGTGTTAGACC; OPN binding site 2 within −2151 to −1735, TGTGTGTGTGTGCGTTT replaced by TTTGCGTGTGTGTGT; FAM129A binding site within −1588 to −906, GGGGTGTGTGGGAAA replaced by AAAGGGTGTGTGGGG; UPP1 binding site 1 within −417 to −238, TAAACACAA replaced by AACACAAAT; UPP1 binding site 2 within −2288 to −1864, TGACCTCAG replaced by GACTCCAGT) were generated by site-specific mutagenesis using the MutanBEST Kit (Takara); and transfected as controls.

To test the direct binding of miR-143/145 to the target gene CBFβ, the whole human CBFβ 3′-UTR sequence was

amplified by PCR using a human genomic DNA template made from HCT116 cells. The PCR products were inserted into the p-MIR-reporter plasmid (Invitrogen). The reverse primer sequence for the CBFβ 3′-UTR was 5′-CCCAAGCTTTGGCAAAAGCAATCTGGTA-3′, and the forward primer sequence was 5′-TGGACTAGTT GACTGATGAGGGAGGTGTT-3′. Efficient insertion was confirmed by sequencing. This construct was cotransfected into HCT116 or SW480 cells with miR-143/145 mimics or inhibitors (pre-miR-143/145 or anti-miR-143/145) and scramble control (Life Technologies). The binding site mutants [binding site 1, GTCACGAAGTAGAG (miR-143)/GACCCTTTTGACCT (miR-145) replaced by GAGATGAAGCACTG (miR-143)/TCCAGTTTTCCCAG (miR-145); binding site 2, AAGTAGAG (miR-143)/ TTTGACCT (miR-145) replaced by GAGATGAA (miR-143)/TCCAGTTT (miR-145)] were also transfected as a control.

For the luciferase reporter assay, the plasmid encoding β-gal was cotransfected and used for normalization. Cells were lysed to measure luciferase activity 24 h after transfection using luciferase assay kits (Promega). Each transfection experiment was performed in triplicate.

Establishment of a mouse CRC xenograft model

Four-week-old athymic BALB/c male nude (nu/nu) mice at 16–18 g were obtained from the Laboratory Animal Center of Nanjing University (Nanjing, China) and maintained under pathogen-limited conditions. The animal experiment was approved by the Medical Ethics Committee of the Nanjing University (IACUC-2006011). All animals received care according to the Guidelines for the Care and Use of Laboratory Animals published by the National Institutes of Health. The animals were randomly and blindly divided into four groups (seven mice per group) and injected subcutaneously into their left flanks with 5×10^6 viable HCT116 cells that stably overexpressed CBFβ (CBFβ-LV) or knocked down CBFβ (shRNA-CBFβ-LV) or the negative control plasmids (Control-LV and shRNA-Control-LV). Subcutaneous tumors were measured on days 9, 12, 15, 18, 21, 24, 27, and 30. The tumor volume was calculated as $½LW^2$, where W and L are the smallest and the largest perpendicular tumor diameters, respectively. The mice were sacrificed at 30 days post implantation, and xenograft tumors were excised, photographed, and weighed.

Establishment of a mouse CRC liver metastasis model

The mouse metastasis model of colorectal cancer was established following a previously described method [51].

Mice were randomly divided into four groups (seven mice per group). To determine metastatic capacity, HCT116 cells that stably overexpressed or downregulated CBFβ or their control cells were injected into the spleens of nude mice. Briefly, mice were anesthetized by peritoneal injection of pentobarbital sodium (40 mg/kg). Through a 1-cm incision in the upper left lateral abdomen, the spleen was accessed through the wound. Then, 2×10^6 cells in vehicle (50 μl) were injected into the distal tip of the spleen with a Hamilton syringe, and the incision was subsequently closed with staples. After 5 weeks, the animals were sacrificed, and the spleens and livers were removed. Micrometastases were statistically evaluated, and liver/spleen sections were stained with H&E.

Statistical analysis

Generally accepted sample sizes were used, with a significant difference between conditions, indicating that the sample size is sufficient. Samples/animals were randomly allocated. The results are expressed as the mean ± standard error. Data were statistically analyzed using Prism software (GraphPad Software Inc. La Jolla, CA, USA) and assessed for normality of distribution using the Shapiro–Wilk test. Differences between multiple groups were compared using one-way ANOVA with Dunnett's tests or, if appropriate, using one-way ANOVA with post hoc Bonferroni correction. Differences between two groups were evaluated using the two-tailed Student's t test. The homogeneity of variance between the two groups were compared against each other in pairs. χ^2 tests were used to analyze the relationship between CBFβ expression and the clinicopathological parameters of patients. Spearman's rank correlation test was used to determine the correlation between the expression of miR-143/miR-145 and CBFβ in CRC patients. A value of $p < 0.05$ was considered statistically significant; ns, not significant.

Data availability

All datasets on which the conclusions of the paper rely are available to readers. The raw data for transcriptome sequencing and ChIP-seq can be accessible at NCBI Gene Expression Omnibus (GEO accession number GSE154876).

Compliance with ethical standards

Conflict of interest The authors declare no competing interests.

Ethics approval and consent to participate Refer to clinical samples and mouse model establishment paragraphs in "Materials and methods."

Publisher's note Springer Nature remains neutral with regard to jurisdictional claims in published maps and institutional affiliations.

References

1. Siegel RL, Miller KD, Goding Sauer A, Fedewa SA, Butterly LF, Anderson JC, et al. Colorectal cancer statistics, 2020. CA Cancer J Clin. 2020;70:145–64.
2. Dienstmann R, Vermeulen L, Guinney J, Kopetz S, Tejpar S, Tabernero J. Consensus molecular subtypes and the evolution of precision medicine in colorectal cancer. Nat Rev Cancer. 2017; 17:79–92.
3. Walther A, Johnstone E, Swanton C, Midgley R, Tomlinson I, Kerr D. Genetic prognostic and predictive markers in colorectal cancer. Nat Rev Cancer. 2009;9:489–99.
4. Xie B, Bai B, Xu Y, Liu Y, Lv Y, Gao X, et al. Tumor-suppressive function and mechanism of HOXB13 in right-sided colon cancer. Signal Transduct Target Ther. 2019;4:51.
5. Su L, Luo Y, Yang Z, Yang J, Yao C, Cheng F, et al. MEF2D transduces microenvironment stimuli to ZEB1 to promote epithelial-mesenchymal transition and metastasis in colorectal cancer. Cancer Res. 2016;76:5054–67.
6. Yan J, Liu Y, Lukasik SM, Speck NA, Bushweller JH. CBFbeta allosterically regulates the Runx1 Runt domain via a dynamic conformational equilibrium. Nat Struct Mol Biol. 2004;11:901–6.
7. Miller J, Horner A, Stacy T, Lowrey C, Lian JB, Stein G, et al. The core-binding factor beta subunit is required for bone formation and hematopoietic maturation. Nat Genet. 2002;32:645–9.
8. Speck NA, Gilliland DG. Core-binding factors in haematopoiesis and leukaemia. Nat Rev Cancer. 2002;2:502–13.
9. Mendoza-Villanueva D, Deng W, Lopez-Camacho C, Shore P. The Runx transcriptional co-activator, CBFbeta, is essential for invasion of breast cancer cells. Mol Cancer. 2010;9:171.
10. Davis JN, Rogers D, Adams L, Yong T, Jung JS, Cheng B, et al. Association of core-binding factor beta with the malignant phenotype of prostate and ovarian cancer cells. J Cell Physiol. 2010;225:875–87.
11. Blyth K, Cameron ER, Neil JC. The RUNX genes: gain or loss of function in cancer. Nat Rev Cancer. 2005;5:376–87.
12. Ito Y, Bae SC, Chuang LS. The RUNX family: developmental regulators in cancer. Nat Rev Cancer. 2015;15:81–95.
13. Gupta S, Ito T, Alex D, Vanderbilt CM, Chang JC, Islamdoust N, et al. RUNX2 (6p21.1) amplification in osteosarcoma. Hum Pathol. 2019;94:23–28.
14. Kayed H, Jiang X, Keleg S, Jesnowski R, Giese T, Berger MR, et al. Regulation and functional role of the Runt-related transcription factor-2 in pancreatic cancer. Br J Cancer. 2007;97:1106–15.
15. Blyth K, Vaillant F, Hanlon L, Mackay N, Bell M, Jenkins A, et al. Runx2 and MYC collaborate in lymphoma development by suppressing apoptotic and growth arrest pathways in vivo. Cancer Res. 2006;66:2195–201.
16. Yi H, Li G, Long Y, Liang W, Cui H, Zhang B, et al. Integrative multi-omics analysis of a colon cancer cell line with heterogeneous Wnt activity revealed RUNX2 as an epigenetic regulator of EMT. Oncogene. 2020;39:5152–64.
17. Sase T, Suzuki T, Miura K, Shiiba K, Sato I, Nakamura Y, et al. Runt-related transcription factor 2 in human colon carcinoma: a potent prognostic factor associated with estrogen receptor. Int J Cancer. 2012;131:2284–93.
18. Wang L, Brugge JS, Janes KA. Intersection of FOXO- and RUNX1-mediated gene expression programs in single breast epithelial cells during morphogenesis and tumor progression. Proc Natl Acad Sci U S A. 2011;108:E803–12.
19. Fijneman RJ, Anderson RA, Richards E, Liu J, Tijssen M, Meijer GA, et al. Runx1 is a tumor suppressor gene in the mouse gastrointestinal tract. Cancer Sci. 2012;103:593–9.
20. Li QL, Ito K, Sakakura C, Fukamachi H, Inoue K, Chi XZ, et al. Causal relationship between the loss of RUNX3 expression and gastric cancer. Cell. 2002;109:113–24.
21. Tanaka S, Shiraha H, Nakanishi Y, Nishina S, Matsubara M, Horiguchi S, et al. Runt-related transcription factor 3 reverses epithelial-mesenchymal transition in hepatocellular carcinoma. Int J Cancer. 2012;131:2537–46.
22. Soong R, Shah N, Peh BK, Chong PY, Ng SS, Zeps N, et al. The expression of RUNX3 in colorectal cancer is associated with disease stage and patient outcome. Br J Cancer. 2009;100:676–9.
23. Ito K, Lim AC, Salto-Tellez M, Motoda L, Osato M, Chuang LS, et al. RUNX3 attenuates beta-catenin/T cell factors in intestinal tumorigenesis. Cancer Cell. 2008;14:226–37.
24. Lee CW, Ito K, Ito Y. Role of RUNX3 in bone morphogenetic protein signaling in colorectal cancer. Cancer Res. 2010;70: 4243–52.
25. Tang YY, Shi J, Zhang L, Davis A, Bravo J, Warren AJ, et al. Energetic and functional contribution of residues in the core binding factor beta (CBFbeta) subunit to heterodimerization with CBFalpha. J Biol Chem. 2000;275:39579–88.
26. Zhen T, Cao Y, Ren G, Zhao L, Hyde RK, Lopez G, et al. RUNX1 and CBFbeta-SMMHC transactivate target genes together in abnormal myeloid progenitors for leukemia development. Blood. 2020;136:2373–85.
27. Ran R, Harrison H, Syamimi Ariffin N, Ayub R, Pegg HJ, Deng W, et al. A role for CBFbeta in maintaining the metastatic phenotype of breast cancer cells. Oncogene. 2020;39:2624–37.
28. Seo W, Shimizu K, Kojo S, Okeke A, Kohwi-Shigematsu T, Fujii SI, et al. Runx-mediated regulation of CCL5 via antagonizing two enhancers influences immune cell function and anti-tumor immunity. Nat Commun. 2020;11:1562.
29. Medema JP, Vermeulen L. Microenvironmental regulation of stem cells in intestinal homeostasis and cancer. Nature. 2011;474:318–26.
30. He XC, Zhang J, Tong WG, Tawfik O, Ross J, Scoville DH, et al. BMP signaling inhibits intestinal stem cell self-renewal through suppression of Wnt-beta-catenin signaling. Nat Genet. 2004;36:1117–21.
31. Wei R, Wong JPC, Lyu P, Xi X, Tong O, Zhang SD, et al. In vitro and clinical data analysis of Osteopontin as a prognostic indicator in colorectal cancer. J Cell Mol Med. 2018;22:4097–105.
32. Rangaswami H, Bulbule A, Kundu GC. Osteopontin: role in cell signaling and cancer progression. Trends Cell Biol. 2006;16:79–87.
33. Wai PY, Mi Z, Guo H, Sarraf-Yazdi S, Gao C, Wei J, et al. Osteopontin silencing by small interfering RNA suppresses in vitro and in vivo CT26 murine colon adenocarcinoma metastasis. Carcinogenesis. 2005;26:741–51.

34. Ishigamori R, Komiya M, Takasu S, Mutoh M, Imai T, Takahashi M. Osteopontin deficiency suppresses intestinal tumor development in Apc-deficient Min mice. Int J Mol Sci 2017;18:1058.

35. Uhlen M, Fagerberg L, Hallstrom BM, Lindskog C, Oksvold P, Mardinoglu A, et al. Proteomics. Tissue-based map of the human proteome. Science. 2015;347:1260419.

36. Yuki R, Aoyama K, Kubota S, Yamaguchi N, Kubota S, Hasegawa H, et al. Overexpression of zinc-finger protein 777 (ZNF777) inhibits proliferation at low cell density through down-regulation of FAM129A. J Cell Biochem. 2015;116:954–68.

37. Roosild TP, Castronovo S, Fabbiani M, Pizzorno G. Implications of the structure of human uridine phosphorylase 1 on the development of novel inhibitors for improving the therapeutic window of fluoropyrimidine chemotherapy. BMC Struct Biol. 2009;9:14.

38. Bhasin N, Alleyne D, Gray OA, Kupfer SS. Vitamin D regulation of the uridine phosphorylase 1 gene and uridine-induced DNA damage in colon in African Americans and European Americans. Gastroenterology. 2018;155:1192–204.e9.

39. Katsumata K, Tomioka H, Sumi T, Yamashita S, Takagi M, Kato F, et al. Correlation between clinicopathologic factors and kinetics of metabolic enzymes for 5-fluorouracil given to patients with colon carcinoma by two different dosage regimens. Cancer Chemother Pharm. 2003;51:155–60.

40. Inokuchi M, Uetake H, Shirota Y, Yamada H, Tajima M, Sugihara K. Gene expression of 5-fluorouracil metabolic enzymes in primary colorectal cancer and corresponding liver metastasis. Cancer Chemother Pharm. 2004;53:391–6.

41. Chen X, Guo X, Zhang H, Xiang Y, Chen J, Yin Y, et al. Role of miR-143 targeting KRAS in colorectal tumorigenesis. Oncogene. 2009;28:1385–92.

42. Pichler M, Ress AL, Winter E, Stiegelbauer V, Karbiener M, Schwarzenbacher D, et al. MiR-200a regulates epithelial to mesenchymal transition-related gene expression and determines prognosis in colorectal cancer patients. Br J Cancer. 2014;110: 1614–21.

43. Sun D, Wang C, Long S, Ma Y, Guo Y, Huang Z, et al. C/EBP-beta-activated microRNA-223 promotes tumour growth through targeting RASA1 in human colorectal cancer. Br J Cancer. 2015; 112:1491–1500.

44. Choi YW, Song YS, Lee H, Yi K, Kim YB, Suh KW, et al. MicroRNA expression signatures associated with BRAF-mutated versus KRAS-mutated colorectal cancers. Medicine. 2016;95:e3321.

45. Cui H, Liu Y, Jiang J, Liu Y, Yang Z, Wu S, et al. IGF2-derived miR-483 mediated oncofunction by suppressing DLC-1 and associated with colorectal cancer. Oncotarget. 2016;7:48456–66.

46. Wang L, Yu P. miR-300 promotes proliferation and EMT-mediated colorectal cancer migration and invasion by targeting p53. Oncol Rep. 2016;36:3225–32.

47. Lin KY, Zhang XJ, Feng DD, Zhang H, Zeng CW, Han BW, et al. miR-125b, a target of CDX2, regulates cell differentiation through repression of the core binding factor in hematopoietic malignancies. J Biol Chem. 2011;286:38253–63.

48. Baffa R, Fassan M, Volinia S, O'Hara B, Liu CG, Palazzo JP, et al. MicroRNA expression profiling of human metastatic cancers identifies cancer gene targets. J Pathol. 2009;219:214–21.

49. Wang C, Zhou X, Li W, Li M, Tu T, Ba X, et al. Macrophage migration inhibitory factor promotes osteosarcoma growth and lung metastasis through activating the RAS/MAPK pathway. Cancer Lett. 2017;403:271–9.

50. Zhang Y, Liu T, Meyer CA, Eeckhoute J, Johnson DS, Bernstein BE, et al. Model-based analysis of ChIP-Seq (MACS). Genome Biol. 2008;9:R137.

51. Hur K, Toiyama Y, Okugawa Y, Ide S, Imaoka H, Boland CR, et al. Circulating microRNA-203 predicts prognosis and metastasis in human colorectal cancer. Gut. 2017;66:654–65.